Instrument Science Report WFC3 2009-37

WFC3 SMOV Programs 11437/9: IR On-orbit PSF Evaluation

G. F. Hartig
10 November 2009

ABSTRACT

We have assessed the image quality of the WFC3 IR channel on orbit, following its alignment to the HST OTA. Point spread function measurements of ~130 stars over the field were made in the F098M, F105W and F160W and compared to model computations and CEI specifications. Deep, core-saturated images of a standard star, sampling the field at 5 locations, were also obtained to evaluate the PSF wings. All encircled energy specifications are met or exceeded, with exception of the inner core EE at 160 nm, as expected from previous ground testing and modeling results. The optical model has been correlated to the observed PSF properties and may be used to predict performance over the full IR spectral range.

Introduction

We have previously discussed measurements of the IR PSF over the field, through three filters spanning the spectral range, in thermal-vacuum tests with the instrument in its final flight configuration (Hartig 2008a). The image quality and wavefront error (Hartig 2008b) were generally found to be excellent, but modeling was required to extend the ground measurements with the CASTLE stimulus to the on-orbit configuration with the HST OTA.

Following alignment of the IR channel to the OTA (involving adjustment of the corrector mechanism to bring the images into focus and optimize the pupil alignment, thereby minimizing the coma that results from pupil shear), a set of confirmatory images were obtained during the SMOV4 campaign to evaluate the optical performance and verify that specifications were achieved.

Observations

The PSF evaluation data were obtained with two SMOV4 programs, 11437 and 11439, executed on 30 and 31 Jul 2009, respectively. Tables 1 and 2 present the observation details. The IR detector was operated at its nominal temperature, –128C, and nominal gain (2.5 e^-/DN). The target for proposal 11437 is a field in NGC-188, an old astrometric open cluster, chosen to yield a reasonable density of appropriately bright stars to permit accurate

encircled energy measurements while sampling the FOV well with relatively short exposures in both filters. The program 11439 target is GD-153, a photometric standard DA white dwarf, selected for its isolation and brightness, which allow measurement of the PSF wings in reasonable exposures without complications from nearby sources.

Table 1. Prog 11437 IR PSF Evaluation Observation Log

rootname	readout	filter	obs_date	obs_time	exptime	pos-targ
iab601xyq	SPARS25/8	F164N	7/30/2009	5:35:28	152.94	(0.000, 0.000)
iab601y0q	SPARS25/8	F164N	7/30/2009	5:39:03	152.94	(0.542, 0.182)
iab601y2q	SPARS25/8	F164N	7/30/2009	5:42:38	152.94	(0.339, 0.485)
iab601y3q	SPARS25/8	F164N	7/30/2009	6:34:52	152.94	(-0.203, 0.303)
iab601y5q	RAPID/16	F127M	7/30/2009	6:45:04	43.98	(0.000, 0.000)
iab601y6q	RAPID/16	F127M	7/30/2009	6:46:50	43.98	(0.542, 0.182)
iab601y8q	RAPID/16	F127M	7/30/2009	6:59:53	43.98	(0.339, 0.485)
iab601y9q	RAPID/16	F127M	7/30/2009	7:01:39	43.98	(-0.203, 0.303)
iab601ybq	RAPID/8	F160W	7/30/2009	7:14:18	20.53	(0.000, 0.000)
iab601ycq	RAPID/8	F160W	7/30/2009	7:15:56	20.53	(20.000, 0.000)
iab601ydq	RAPID/8	F160W	7/30/2009	7:17:34	20.53	(20.000,20.000)
iab601yeq	RAPID/8	F160W	7/30/2009	7:19:12	20.53	(0.000,20.000)
iab601yjq	RAPID/8	F098M	7/30/2009	8:08:24	20.53	(0.000, 0.000)
iab601ykq	RAPID/8	F098M	7/30/2009	8:10:02	20.53	(20.000, 0.000)
iab601ylq	RAPID/8	F098M	7/30/2009	8:11:40	20.53	(20.000,20.000)
iab601ymq	RAPID/8	F098M	7/30/2009	8:13:18	20.53	(0.000,20.000)
iab601ypq	RAPID/8	F105W	7/30/2009	8:25:57	20.53	(0.000, 0.000)
iab601yqq	RAPID/8	F105W	7/30/2009	8:27:35	20.53	(20.000, 0.000)
iab601yrq	RAPID/8	F105W	7/30/2009	8:29:13	20.53	(20.000,20.000)
iab601ysq	RAPID/8	F105W	7/30/2009	8:30:51	20.53	(0.000,20.000)

Table 2. Prog 11439 IR PSF Wing Evaluation Observation Log

rootname	readout	filter	obs_date	obs_time	exptime	pos-targ
iabl01d7q	STEP100/16	F098M	7/31/2009	3:22:53	899.23	(5.000, 5.000)
iabl01d8q	STEP200/16	F160W	7/31/2009	3:50:47	1599.23	(-5.000, -5.000)
iabla1daq	STEP200/16	F160W	7/31/2009	5:04:48	1599.23	(38.000, 32.000)
iabla1dbq	STEP100/16	F098M	7/31/2009	5:20:50	899.23	(37.000, 31.000)
iablb1ddq	STEP100/16	F098M	7/31/2009	6:28:59	899.23	(38.000,-32.000)
iablb1deq	STEP200/16	F160W	7/31/2009	6:56:41	1599.23	(37.000,-31.000)
iablc1dgq	STEP200/16	F160W	7/31/2009	8:16:30	1599.23	(-38.000,-32.000)
iablc1diq	STEP100/16	F098M	7/31/2009	8:32:32	899.23	(-37.000,-31.000)
iabld1djq	STEP100/16	F098M	7/31/2009	9:40:41	899.23	(-38.000, 32.000)
iabld1dlq	STEP200/16	F160W	7/31/2009	10:08:23	1599.23	(-37.000, 31.000)

POS-TARG offsets were employed to improve field coverage, to avoid blemishes and to ameliorate potential persistence effects in the highly-saturated exposures used to investigate the PSF wings. Substantial persistence results from saturated exposures and can readily be detected in these images. Full frame images were used throughout both programs. The (non-destructive) readout patterns were chosen to sample the PSF core region with exposure depth increasing over several reads to about half full-well for many stars in the field for program 11437, and extended to about 40 times full-well for program 11439. These highly saturated full-frame images were obtained to study the far wings and investigate possible ghosting, stray light, and electronic cross-talk anomalies. Five

pointings, toward each corner of the field and near field center, were used for program 11439; the images are not exactly centered, since the SMOV alignment process required corrector mechanism adjustments that offset the field by ~ 5 arcsec. The images obtained with filters F164N and F127M were dithered with a standard box pattern resulting in less field coverage. These generally have lower signal levels and were added to the program as a test of super-resolution using multi-drizzle, and are not considered further herein.

Analyses

The NGC-188 field images (11437) were analyzed by first identifying suitable stars, which are of sufficient signal level (>3-5 ke^- in the peak px), and isolated from neighbors and field edges, bad pixels, etc. in order to permit accurate encircled energy computation. This selection was accomplished with IDL tool *find_psfs*, which, after automatically selecting suitable PSFs, permits manual inspection of the results, enabling further vetting. The POS-TARG offset fields were independently treated, with results from all fields collated for analysis and plotting.

Measurements of each PSF were made using *wfc3_psf_eval*, which computes the encircled energy (EE) within specified apertures, the FWHM of the best fit 2-D Gaussian (in px), peak pixel fraction, sharpness (sum of the square of the unity-normalized PSF) and ellipticity. Because an aperture of ~2 arcsec radius is used for the computations, the EE and peak fraction values are corrected for the PSF flux outside that aperture, amounting to ~3%, as measured using the PSF wing evaluation data (see below). The sharpness is not sensitive to the PSF wings, but is dominated by the core within a few pixels radius. The OTA breathing model was also used to estimate the telescope focus state at the time of each observation; this is useful for confirmation of the IR corrector focus setting.

Figure 1 displays some measurement results for each selected star in the F098M and F160W images at the appropriate field location. The relative EE within the relevant CEI spec inner core diameter (0.25 arcsec) is indicated by the color, ranging from violet (low) to red (high). Circle diameter indicates the relative sharpness (left) and FWHM (right); the same scale is used for both filters. There is apparent correlation between the core EE and both image width and sharpness, even though the latter are more sensitive to the centration of the PSF with respect to the pixel boundaries. The core EE of the F098M images also demonstrates some left-right field dependence that is not clearly present in the F105W or F160W measurements. The mean core EE within the central inscribed diamond (formed by joining the mid-points of the sides) is nearly identical to that outside the diamond. This has relevance to the CEI spec, which refers to points at mid-field and along the diamond edges.

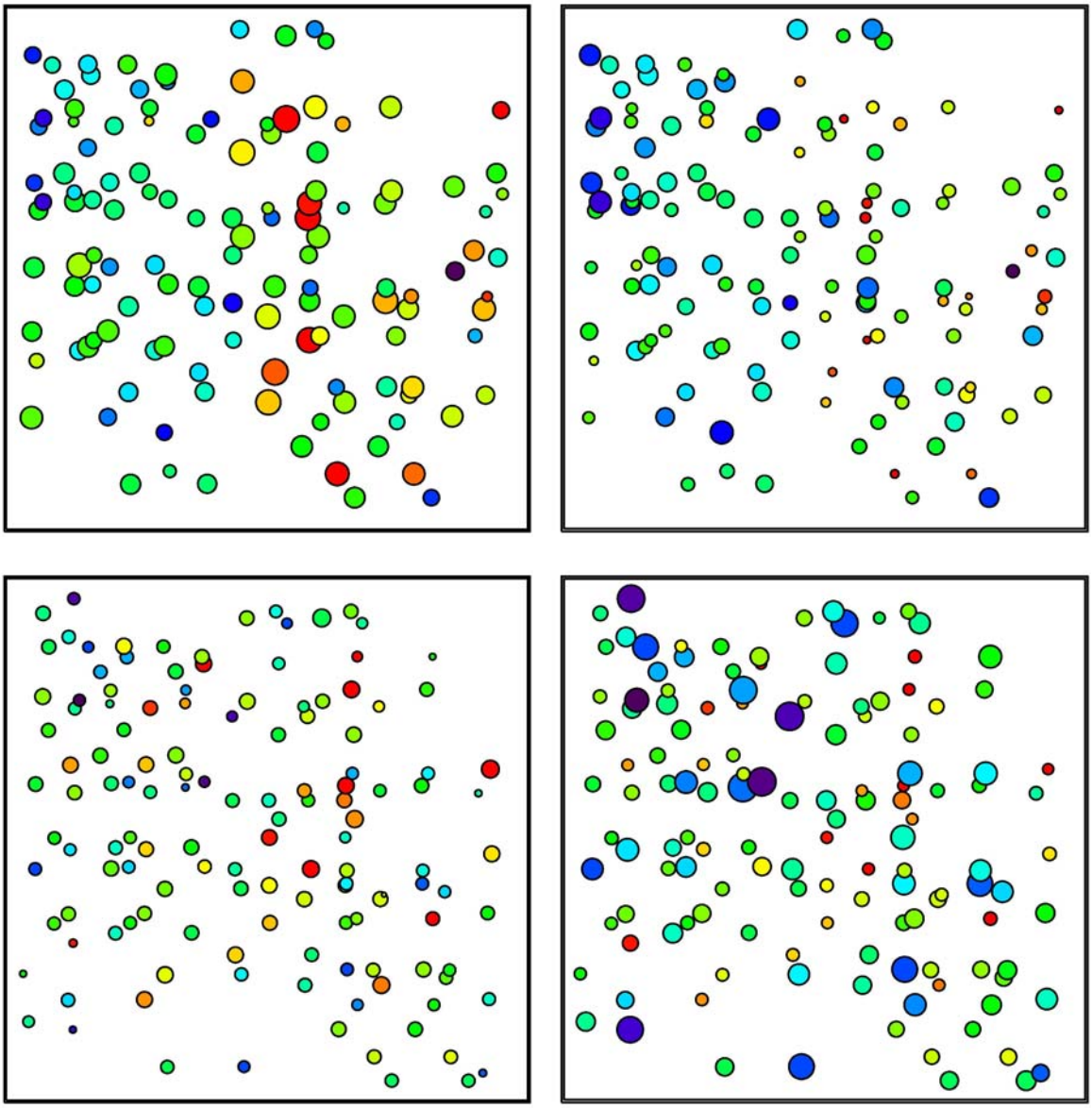

Figure 1. Measured PSF field locations and parameters for selected stars in the Program 11437 images through F098M (top) and F160W (bottom). The relative EE in the PSF core is indicated by the color of the circles, while the relative sharpness (left) and FWHM (right) are indicated by the diameter.

The PSF core measurements for the each of the filters are summarized in Tables 3-5, with their average, range and standard deviation; 130 stars were measured for F098M and 135 for F105W and 134 for F160W. The three EE values listed in the tables are for diameters of 0.25, 0.37, and 0.60 arcsec, the latter two corresponding to the CEI spec outer core EE diameters for 1 and 1.6 μ; the former applies to both wavelengths as the inner core EE diameter. These EE values were measured using regions of the images extending to ~ 2 arcsec in radius; small corrections for the ~3% of the PSF flux outside that radius have been applied. Comparison of these EE values, measured through medium and broadband filters, to the specs at given wavelengths requires some correction, using PSF models, as discussed below.

Table 3. Program 11437 IR F098M PSF Measurement Summary

n=130	EE.25	EE.37	EE.60	shrp	peak	fwhm	ellip
avg:	0.568	0.753	0.847	0.118	0.263	1.280	0.042
min:	0.503	0.697	0.791	0.048	0.139	0.999	0.009
max:	0.626	0.797	0.896	0.170	0.379	1.532	0.066
std:	0.026	0.013	0.012	0.023	0.051	0.115	0.015

Table 4. Program 11437 IR F105W PSF Measurement Summary

n=135	EE.25	EE.37	EE.60	shrp	peak	fwhm	ellip
avg:	0.554	0.740	0.847	0.117	0.264	1.294	0.043
min:	0.497	0.690	0.793	0.061	0.144	0.975	0.012
max:	0.621	0.774	0.885	0.170	0.375	1.603	0.114
std:	0.027	0.012	0.010	0.025	0.056	0.141	0.022

Table 5. Program 11437 IR F160W PSF Measurement Summary

n=134	EE.25	EE.37	EE.60	shrp	peak	fwhm	ellip
avg:	0.477	0.645	0.822	0.084	0.213	1.348	0.035
min:	0.436	0.598	0.770	0.030	0.110	1.151	0.007
max:	0.510	0.690	0.872	0.114	0.293	1.723	0.074
std:	0.016	0.014	0.012	0.015	0.041	0.143	0.016

The program 11439 data were processed by the calwf3 pipeline to produce high dynamic range images for each filter at the five tested field points. Use of the STEP100 and STEP 200 timing patterns permits derivation of the high dynamic range required to assess the PSF wings, with effective exposure time of 900 or 1600 sec, yet sampling the core with several readouts without saturating. This results in images with effective peak pixel signal of ~5 Me^-, and permits evaluation of the azimuthally-averaged PSF wings out to radius >5 arcsec, for comparison with CEI specifications.

Figure 2 is a montage of the central region of the deep PSF images, displayed at their approximate field locations, for each of the two filters with a logarithmic stretch. The images are magnified relative to the field size by a factor 4 and subtend ~6 arcsec. The measured EE within the core spec diameters (0.25 and 0.37 arcsec for 1 μ; 0.25 and 0.6 at 1.6 μ) is shown near each PSF; the variations are judged to be within the measurement uncertainties.

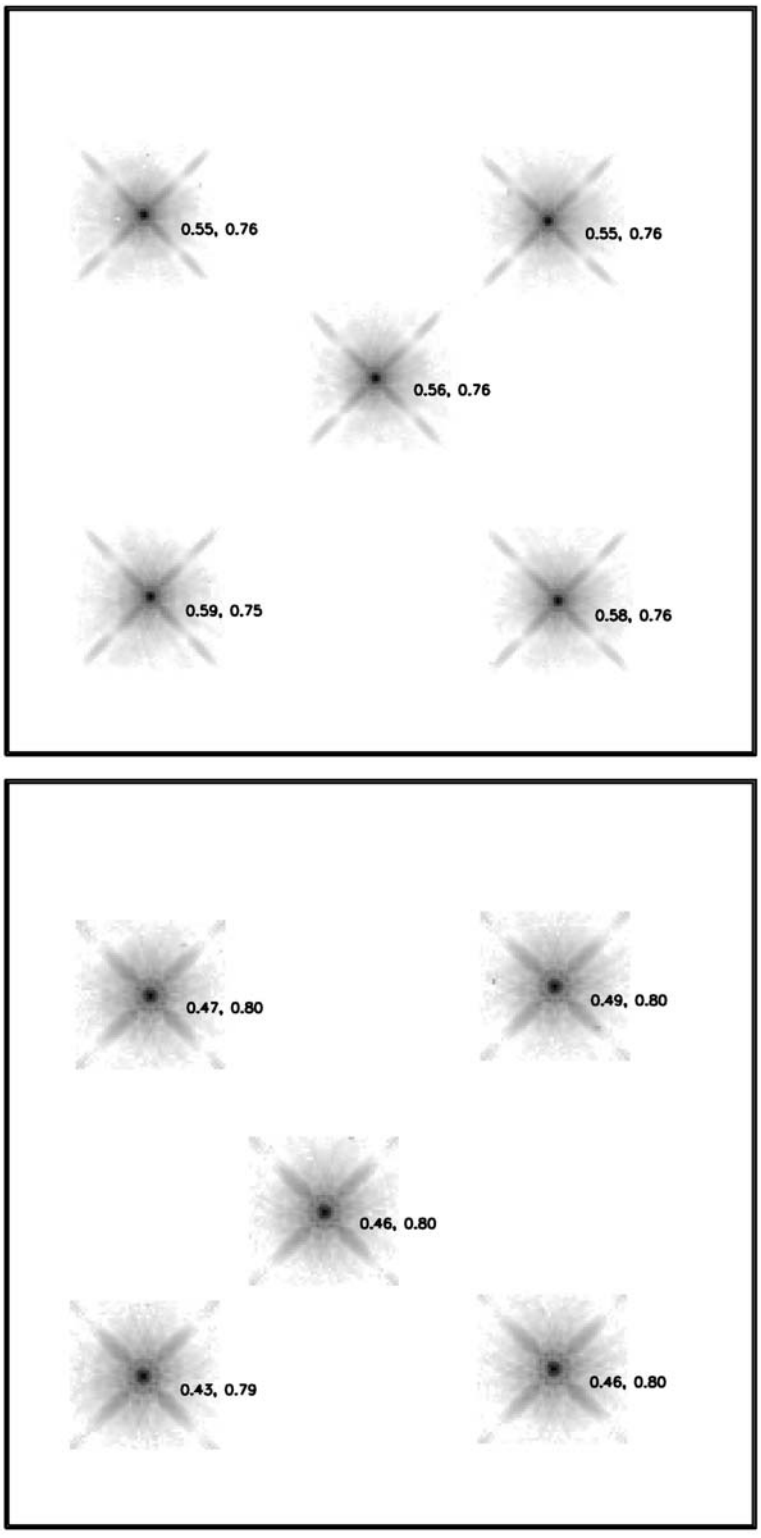

Figure 2 . Montages of measured PSF cores from Program 11439 illustrating their field position for filter F098M (top) and F160W (bottom), displayed with a 5 dex log stretch. The images are magnified by a factor 4 relative to the field and are corrected for geometric distortion. Core EE values within the relevant spec diameters are shown.

Larger versions of the deep images, subtending ~20 arcsec, are shown in Figure 3 for the F098M and F160W exposures near field center. They are not corrected for geometrical distortion, so are visibly elongated along the vertical axis, due to the detector tilt with respect to the chief ray inherent in the IR channel design. Although the target was chosen to be isolated, a number of field galaxies appear in all of the images; some of these galaxies are also seen in the UVIS channel F625W images of the same target (Hartig, 2009). Some detector artifacts, including warm and dead pixels and imperfectly removed cosmic ray hits are also evident. No ghost images are apparent.

For each of the high dynamic range images, the EE and azimuthally-averaged (AA) PSF (fractional flux per pixel) were computed as a function of radius, from ~ 1px to 6 arcsec, and plotted in Figure 4, along with the EE specification values in the core and wings at 1 and 1.6 μ, which are shown as linked crosses. The scatter at small radius is due to the sensitivity of these measurements to PSF centration relative to the pixel boundaries. The wing EE specs are clearly exceeded, in all cases.

Modeling

In order to extrapolate these observed data to other wavelengths, we begin with modeling the measured PSFs using straightforward calculations, including only an assessment of the low order WFE from design and alignment residuals, the OTA pupil geometry, the OTA mirror mid-frequency OPD maps, and a reasonable estimate of the detector MTF, due mostly to inter-pixel capacitance and charge diffusion, which are approximated by convolving the PSF with a Gaussian kernel (Hartig 2008a). The resultant PSFs were then evaluated with the same tools as the measured PSFs and results shown as dotted lines in Figure 4. The agreement between measurement and model is reasonable, from radii of 130 mas (1px) to 6 arcsec. Using this model, we can compute PSFs and measure their relevant characteristics to estimate performance over the full spectral range of the IR channel. Results are listed in tables 6-9.

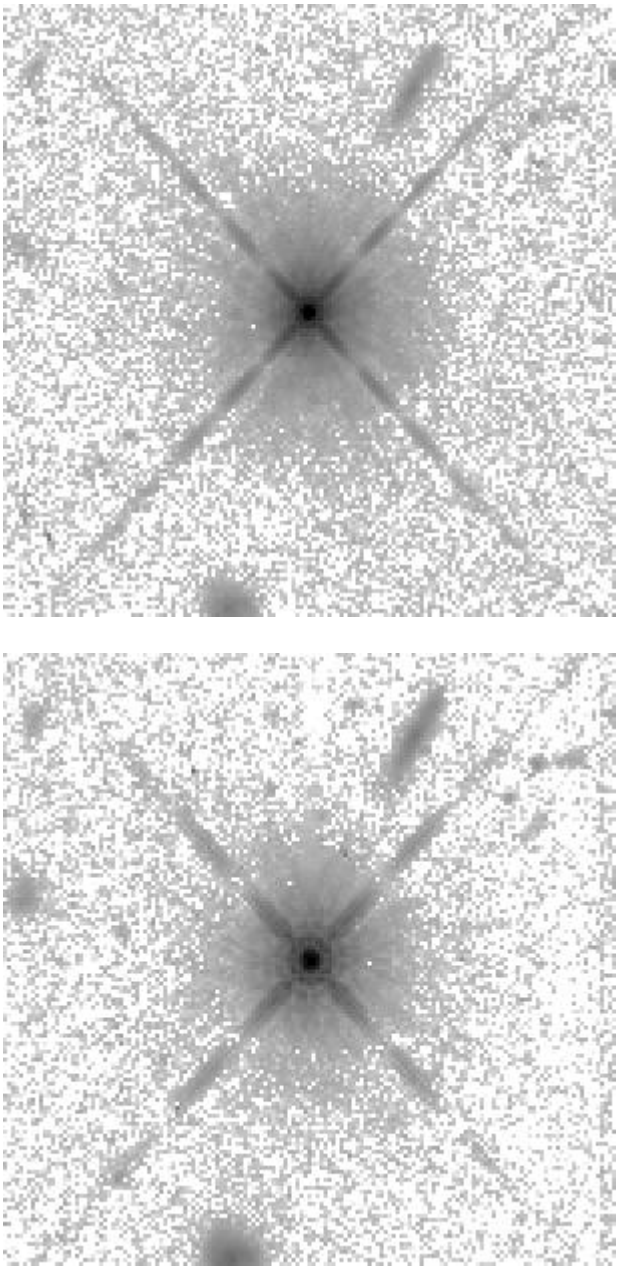

Figure 3 . DeepPSF images near field center from Program 11439 for filter F098M (top) and F160W (bottom) displayed with a 6 dex log stretch. Each image subtends ~20 arcsec on a side and is not distortion-corrected. Several field objects are evident.

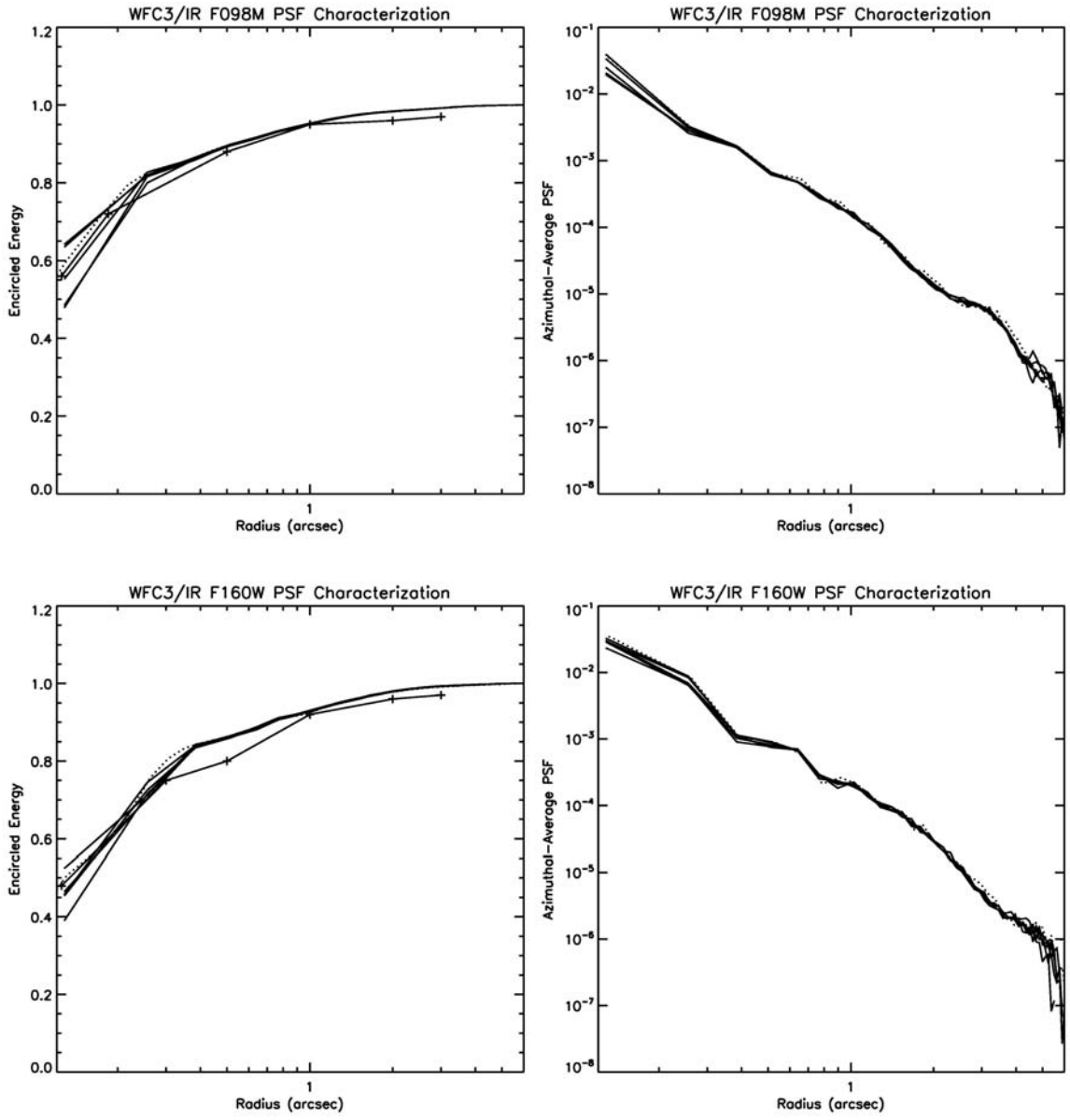

Figure 4 . Encircled energy and azimuthally-averaged PSF (fractional flux per pixel) vs. radius for each of the five deep PSFs from Program 11439 for filter F098M (top) and F160W (bottom). Model shown as dotted line. EE specs are connected crosses.

Table 6. On-orbit IR PSF Model Encircled Energy vs. Radius Estimates

λ(μ):	0.7	0.8	0.9	1.0	1.1	1.2	1.3	1.4	1.5	1.6	1.7
0.10	0.575	0.549	0.524	0.502	0.484	0.468	0.453	0.438	0.426	0.410	0.394
0.15	0.736	0.714	0.685	0.653	0.623	0.596	0.575	0.558	0.550	0.539	0.531
0.20	0.802	0.794	0.780	0.762	0.739	0.712	0.683	0.653	0.631	0.608	0.590
0.25	0.831	0.827	0.821	0.813	0.804	0.792	0.776	0.756	0.735	0.708	0.679
0.30	0.850	0.845	0.838	0.833	0.828	0.822	0.816	0.808	0.803	0.789	0.770
0.40	0.878	0.876	0.869	0.859	0.850	0.845	0.841	0.838	0.840	0.836	0.832
0.50	0.899	0.894	0.889	0.884	0.878	0.868	0.858	0.852	0.854	0.850	0.848
0.60	0.916	0.913	0.904	0.897	0.893	0.889	0.883	0.875	0.870	0.863	0.859
0.80	0.937	0.936	0.929	0.924	0.918	0.909	0.903	0.900	0.903	0.900	0.895
1.00	0.951	0.951	0.946	0.941	0.935	0.930	0.925	0.920	0.917	0.912	0.909
1.50	0.967	0.969	0.967	0.965	0.963	0.959	0.954	0.951	0.952	0.948	0.943
2.00	0.974	0.977	0.976	0.975	0.973	0.972	0.969	0.967	0.970	0.967	0.963

Table 7. On-orbit IR PSF Model Ensquared Energy Estimates

λ(μ):	0.7	0.8	0.9	1.0	1.1	1.2	1.3	1.4	1.5	1.6	1.7
1	0.435	0.417	0.398	0.381	0.365	0.348	0.331	0.314	0.299	0.283	0.267
2	0.728	0.707	0.679	0.648	0.618	0.592	0.571	0.554	0.545	0.534	0.524
3	0.815	0.811	0.802	0.790	0.776	0.757	0.733	0.706	0.682	0.655	0.631
5	0.872	0.868	0.858	0.849	0.844	0.840	0.836	0.830	0.830	0.826	0.821
7	0.905	0.900	0.894	0.888	0.882	0.872	0.862	0.855	0.856	0.854	0.852
9	0.927	0.924	0.917	0.909	0.904	0.898	0.893	0.888	0.886	0.876	0.868
11	0.941	0.939	0.934	0.928	0.921	0.914	0.910	0.905	0.905	0.901	0.897
13	0.951	0.951	0.946	0.941	0.936	0.930	0.924	0.917	0.919	0.915	0.911
15	0.957	0.958	0.955	0.951	0.946	0.942	0.936	0.931	0.931	0.925	0.921
17	0.961	0.963	0.962	0.958	0.955	0.950	0.945	0.942	0.942	0.938	0.933
19	0.964	0.967	0.966	0.964	0.961	0.958	0.954	0.949	0.951	0.947	0.942
21	0.967	0.969	0.969	0.967	0.965	0.963	0.960	0.956	0.957	0.953	0.950
23	0.970	0.972	0.971	0.970	0.969	0.967	0.964	0.961	0.964	0.960	0.956
25	0.972	0.974	0.973	0.972	0.971	0.970	0.968	0.965	0.968	0.965	0.962
51	0.993	0.993	0.991	0.990	0.988	0.987	0.986	0.985	0.988	0.987	0.986
101	0.998	0.999	0.998	0.998	0.997	0.997	0.996	0.996	0.998	0.997	0.997

Table 8. On-orbit IR PSF Model Sharpness Estimates

λ(μ):	0.7	0.8	0.9	1.0	1.1	1.2	1.3	1.4	1.5	1.6	1.7
Ctr'd	0.213	0.197	0.182	0.169	0.156	0.144	0.132	0.121	0.112	0.102	0.093
Corner	0.134	0.127	0.118	0.109	0.100	0.093	0.087	0.083	0.080	0.077	0.074

Table 9. On-orbit IR PSF Model FWHM Estimates

λ(μ):	0.7	0.8	0.9	1.0	1.1	1.2	1.3	1.4	1.5	1.6	1.7
px	0.953	0.971	0.986	1.001	1.019	1.040	1.067	1.100	1.136	1.176	1.219
arcsec	0.122	0.124	0.126	0.128	0.130	0.133	0.137	0.141	0.145	0.151	0.156

Conclusion

We conclude that the on-orbit optical performance of the WFC3 IR channel is generally excellent, as predicted from ground test and analysis. Table 10 lists the relevant CEI specs which we are able to verify with the data described herein, along with their pre-flight predictions and the measured on-orbit values. Because the measurements shown in tables 3 through 5 are made through medium and broadband filters, corrections must be applied to compare these EEs to the spec values at (monochromatic) wavelengths. To determine the corrections, model images were synthesized using the system throughput over each filter bandpass and an assumed stellar SED and compared with monochromatic models. All image quality specs are satisfied, with exception of the inner core EE at 1.6 μ, which falls ~2% below the requirement, as was predicted from ground based tests and modeling (Hartig, 2008a). The measurements are generally close to the predictions, but the modeling required to extrapolate ground performance to that with the OTA is uncertain.

Table 10. On-orbit IR Image Quality (EE) Spec Conformance

λ(μ)	Diam (")	Req	Goal	Predict	Measured
1.0	0.25	0.56	0.61	0.58	0.56
	0.37	0.72	0.80	0.72	0.75
	1.00	0.88		0.89	0.89
	2.00	0.95		0.95	0.95
	4.00	0.96		0.98	0.98
	6.00	0.97		0.99	0.99
1.6	0.25	0.48	0.54	**0.46**	**0.46**
	0.60	0.75	0.80	0.78	0.81
	1.00	0.80		0.85	0.86
	2.00	0.92		0.92	0.93
	4.00	0.96		0.97	0.98
	6.00	0.97		0.99	0.99

We have produced an optical model that produces PSFs in general agreement with the observed field-averaged IR PSF; this model may be used to predict optical performance parameters for purposes of observation planning. A more detailed model, including variation over the field, awaits further analyses.

Acknowledgements

The author is grateful to Linda Dressel for assistance in the instrument optical alignment and for critical reading of this report.

References

Hartig, G.F. “WFC3 IR PSF Evaluation in Thermal-Vacuum Test #3”, STScI ISR WFC3-2008-41, 2008a

Hartig, G.F. “WFC3 Optical Wavefront Error Characterization in Thermal-Vacuum Test #3”, STScI ISR WFC3-2008-31, 2008b.

Hartig, G.F. “WFC3 SMOV Programs 11436/8: IR On-orbit PSF Evaluation”, STScI ISR WFC3-2009-38, 2009.